Title

Geomagnetic intensity variations for the past 8 kyr: New archaeointensity results from Eastern China

Journal

Earth and Planetary Science Letters, 392

ISSN

0012-821X

Authors

Cai, S
Tauxe, L
Deng, C
et al.

Publication Date

2014-04-15

DOI

10.1016/j.epsl.2014.02.030

Peer reviewed

Earth and Planetary Science Letters 392 (2014) 217–229

Contents lists available at ScienceDirect

Earth and Planetary Science Letters

www.elsevier.com/locate/epsl

Geomagnetic intensity variations for the past 8 kyr: New archaeointensity results from Eastern China

Shuhui Cai [a,b,*], Lisa Tauxe [c], Chenglong Deng [a], Yongxin Pan [b], Guiyun Jin [d], Jianming Zheng [e], Fei Xie [f], Huafeng Qin [b], Rixiang Zhu [a]

[a] State Key Laboratory of Lithospheric Evolution, Institute of Geology and Geophysics, Chinese Academy of Sciences, Beijing 100029, China
[b] Key Laboratory of the Earth's Deep Interior, Institute of Geology and Geophysics, Chinese Academy of Sciences, Beijing 100029, China
[c] Scripps Institution of Oceanography, University of California, San Diego, La Jolla, CA 92093-0220, USA
[d] School of History and Culture, Shandong University, Jinan 250100, China
[e] Zhejiang Provincial Institute of Cultural Relics and Archaeology, Hangzhou 310014, China
[f] Hebei Province Institute of Cultural Relics, Shijiazhuang 050000, China

ARTICLE INFO

Article history:
Received 3 August 2013
Received in revised form 9 February 2014
Accepted 12 February 2014
Available online 6 March 2014
Editor: L. Stixrude

Keywords:
archaeointensity
China
regional model of Eastern Asia
non-dipolar moment

ABSTRACT

In this study, we have carried out paleointensity experiments on 918 specimens spanning the last ~7 kyr, including pottery fragments, baked clay and slag, collected from Shandong, Liaoning, Zhejiang and Hebei Provinces in China. Approximately half of the specimens yielded results that passed strict data selection criteria and give high-fidelity paleointensities. The virtual axial dipole moments (VADMs) of our sites range from $\sim 2 \times 10^{22}$ to $\sim 13 \times 10^{22}$ Am^2. At ~2250 BCE our results suggest a paleointensity low of $\sim 2 \times 10^{22}$ Am^2, which increases to a high of $\sim 13 \times 10^{22}$ Am^2 by ~1300 BCE. This rapid (less than 1000 yrs) six-fold change in the paleointensity may have important implications for the dynamics of core flow at this time. Our data from the last ~3 kyr are generally in good agreement with the ARCH3k.1 model, but deviate significantly at certain time periods from the CALS3k.4 and CALS10k.1b model, which is likely due to differences in the data used to constrain these models. At ages older than ~3 ka, where only the CALS10k.1b model is available for comparison, our data deviate significantly from the model. Combining our new results with the published data from China and Japan, we provide greatly improved constraints for the regional model of Eastern Asia. When comparing the variations of geomagnetic field in three global representative areas of Eastern Asia, the Middle East and Southern Europe, a common general trend of sinusoidal variations since ~8 ka is shown, likely dominated by the dipole component. However, significant disparities are revealed as well, which we attribute to non-dipolar components caused by movement of magnetic flux patches at the core-mantle boundary.

1. Introduction

The geomagnetic field is generated by the motion of the Earth's fluid outer core and its variation is driven by the Earth's deep internal dynamics. Therefore, the behavior of geomagnetic field has significant potential to yield insight into Earth's geodynamics, such as the influence of core-mantle interactions (Biggin et al., 2012; Bloxham, 2000), changes in outer-core flow and geomagnetic jerks (Bloxham et al., 2002; Dumberry and Finlay, 2007; Mandea et al., 2010; Olsen and Mandea, 2008). Besides the geodynamic significance, connections between the geomagnetic field and global climate have been suggested (Courtillot et al., 2007; Gallet et al., 2005; Kent, 1982), but these claims remain controversial (Bard and Delaygue, 2008). Furthermore, archaeomagnetic studies focusing on the detailed evolution of the geomagnetic field over the past ~8 kyr have a potential application on archaeomagnetic dating (Ben-Yosef et al., 2008b, 2010; Pavón-Carrasco et al., 2009, 2011).

The geomagnetic field varies over a broad range of timescales. To understand the variation over periods of thousands of years we rely entirely on measurements of remanent magnetization from geological and archaeological materials. Archaeomagnetic data from Eastern Asia, however, are sparse, particularly those that would be widely regarded as reliable (Yu, 2012). The main archaeomagnetic work in China was carried out in the 1980s and 1990s (Huang et al., 1998; Shaw et al., 1995, 1999; Tang et al., 1991; Wei et al., 1982, 1986, 1987) and published data are rather

* Corresponding author at: Institute of Geology and Geophysics, Chinese Academy of Sciences, 19 Bei-Tu-Cheng-Xi-Lu, Beijing 100029, China. Tel.: +86 (10) 8299 8418; fax: +86 (10) 6201 0846.
E-mail address: shuhui.cai08@gmail.com (S. Cai).

http://dx.doi.org/10.1016/j.epsl.2014.02.030
0012-821X/

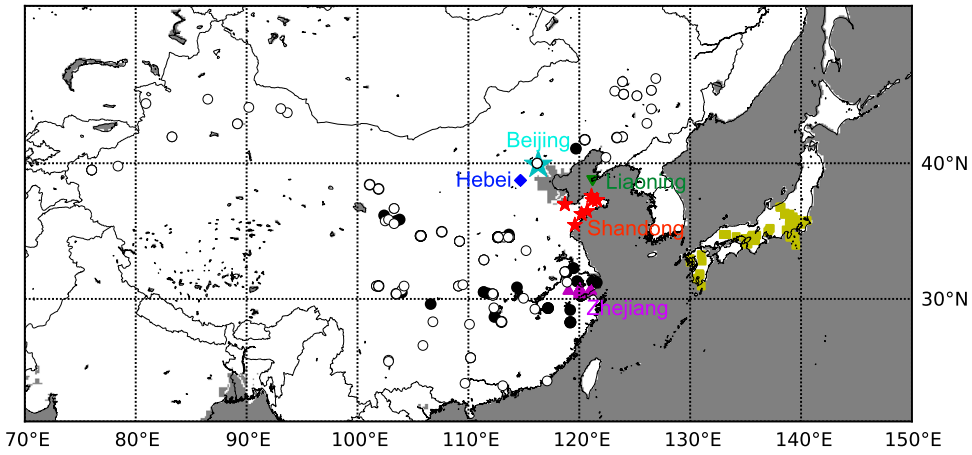

Fig. 1. Distributions of archaeomagnetic sites in China and Japan. Black solid/open circles represent locations of the accepted/rejected archaeointensity data in China from GEOMAGIA50 database. Red stars/green triangles down/magenta triangles/blue diamonds represent Shandong/Liaoning /Zhejiang/Hebei locations in this study. Yellow squares represent the accepted published data in Japan from GEOMAGIA50 database. Data selection criteria please see the text. (For interpretation of the references to color in this figure legend, the reader is referred to the web version of this article.)

scattered (Fig. S1). The scatter might reflect genuine rapid changes in the geomagnetic field, or inaccuracies in age models, poor data quality (Table S1) caused by lack of modern experiment technique and loose selection criteria or a combination of these. The longevity of Chinese civilization and the abundant nature of archaeological artifacts make archaeomagnetic studies within China an important tool for filling in many gaps in our current data sets. This archaeointensity study was carried out on archaeological artifacts from four locations in China spanning the past ~7 kyr.

2. Sampling background

The artifacts used in this study were collected from four different provinces of Shandong, Liaoning, Zhejiang and Hebei, which are located at eastern China (Fig. 1). The archaeological structures cover living sites, saltern and kilns (Table 1) with materials varying from baked clay, pottery, porcelain to slag, spanning the past ~7 kyr (Fig. 2). Because of the lack of materials suitable for radiocarbon dating, all the dating here is based on archaeological estimates according to historic documents and pottery characteristics. In this paper, each province is treated as a paleomagnetic location, made up of multiple archaeological sites excavated at various times. While a paleomagnetic 'site' is defined as a single time horizon, the term in archaeology refers to independent excavations. We use the term in the archaeological context here. 'Sample' here refers to a discrete piece of material, such as a pottery fragment or brick, while 'specimens' are different fragments from a sample. Since samples from one archaeological 'site' might have different ages, we use sample level averages in the discussion in this study. The site name is generally derived from an abbreviation of archaeological site, for example, BQ represents samples from the Bei-Qian site. We use lower case letters and terminal digits to distinguish different samples and specimens separately. For instance, BQa-01 means the first specimen from sample 'a' of site BQ.

2.1. Samples from Shandong and Liaoning provinces

Most of the samples from Shandong province were first collected by archaeologists during an archaeological survey or excavation prior to archaeomagnetic sampling, except for two samples from Shouguang city, which were collected *in situ*. The two samples from Liaoning province were collected together with the samples from Shandong and were not *in situ*. In some cases, only one sample is obtained from a site and we use the single sample to represent the site level because of either the unexceptionable behavior of the sample during the paleointensity experiment (YJC) or consistent results with data from other sites of the same age (GJC). These artifacts cover 5 areas in Shandong and 1 in Liaoning, which include 10 archaeological sites in total and span from early Dawenkou culture (5000–4000 BCE) to Song-Yuan dynasty (960–1368 CE). The archaeological structures are mainly living sites belonging to prehistoric culture, which are generally excavated in order to rescue the ancient relics exposed by construction projects.

2.2. Samples from Zhejiang province

Deqing county, situated in Huzhou city, Zhejiang province, is considered to be the cradle of protoporcelain (transition from pottery to porcelain). Many ancient kilns were found in this area during archaeological surveys. In this study, 11 archaeological sites are included, most of which were collected from or nearby Deqing county and thus all are named DQ for simplicity. DQ1–DQ6 were collected by archaeologists during a survey and preserved in the Deqing museum while DQ7–DQ11 were sampled *in situ*. Since most of the artifacts were collected from the ground surface at the unexcavated sites (only DQ10 is in excavation), stratigraphic information is not available. These materials span ~2500 yrs from Shang dynasty (16th–11th Century BCE) to early Tang dynasty (618–763 CE).

2.3. Samples from Hebei province

Dingyao site is one of the most famous kiln sites in northern China. It is located 25 km north of Quyang county, Hebei province, and is well known for its white porcelain. This kiln site comprises a group of kilns spanning ~600 yrs, starting in the Tang dynasty and reaching a peak in activity during the Song dynasty followed by a decline during the Jin-Yuan dynasty. Three excavations were conducted here and dozens of kilns were exposed. Samples from these sites are mainly porcelain fragments spanning the middle-late Tang dynasty (763–907 CE) to the Yuan dynasty (1271–1368 CE) recovered from five independent excavations. DY1–DY4 were supplied to us by archaeologists from archived materials while DY5–DY24 were collected from a unit originally excavated in 1985, DY25–DY33 from a unit excavated in 2009, DY34–DY37 from a kiln used during the Jin dynasty, DY38–DY40 from Beizhen kiln site and DY41–DY42 from a pile of debris at Jiancixi. These units are so close to each other that they have a limited difference of latitude and longitude.

Table 1
Sample information analyzed in this study. Dating is based on archaeological background. Lat/Lon: latitude/longitude; N/n: number of samples/specimens.

Site	Epoch	Age	Lat/°N	Lon/°E	Structure	Material	N/n
Qingdao, Shandong							
BQ	Early Dawenkou Culture	4000 ± 500 BCE	36.60	120.70	Living site	Baked clay	2/15
Yantai, Shandong							
DZJ	Early Dawenkou Culture	4000 ± 500 BCE	37.70	121.10	Living site	Pottery	5/16
QJZ	Early Dawenkou Culture	4000 ± 500 BCE	37.40	121.20	Living site	Pottery	4/13
GDD	Early Dawenkou Culture	4500 ± 500 BCE	37.40	121.60	Living site	Pottery	5/23
XJT	Early Dawenkou Culture	4000 ± 500 BCE	37.40	121.60	Living site	Pottery	5/25
Rizhao, Shandong							
LCZ	Longshan Culture	2250 ± 250 BCE	35.60	119.60	Living site	Pottery	4/23
Jiaozhou, Shandong							
ZJZ	Longshan Culture	2250 ± 250 BCE	36.40	120.20	Living site	Pottery	4/25
Shouguang, Shandong							
SWC4	Song-Yuan Dynasty	1164 ± 204 CE	37.10	118.70	Saltern	Pottery	2/11
SWC5	Late Shang Dynasty	1150 ± 150 BCE	37.10	118.70	Saltern	Pottery	2/15
Dalian, Liaoning							
YJC	Yueshi Culture	1800 ± 200 BCE	38.90	121.20	Living site	Baked clay	1/10
GJC	Longshan Culture	2250 ± 250 BCE	38.90	121.20	Living site	Pottery	1/5
Huzhou, Zhejiang							
DQ1	Middle-Late Chunqiu Dynasty	550 ± 74 BCE	30.62	120.02	Kiln	Pottery	3/15
DQ2	Middle-Late Chunqiu Dynasty	550 ± 74 BCE	30.62	119.03	Kiln	Pottery	1/10
DQ3	Donghan Dynasty	123 ± 98 CE	30.51	120.00	Kiln	Pottery	3/20
DQ4	Early Tang Dynasty	691 ± 73 CE	30.63	120.07	Kiln	Pottery	3/15
DQ5	Dongjin-Nanchao Dynasty	453 ± 136 CE	30.36	120.02	Kiln	Pottery	4/25
DQ6	Early Chunqiu Dynasty	697 ± 74 BCE	30.59	120.01	Kiln	Pottery	2/15
DQ7	Zhanguo Dynasty	348 ± 127 BCE	30.62	120.02	Kiln	Pottery, Baked clay	18/72
DQ8	Zhanguo Dynasty	348 ± 127 BCE	30.61	121.02	Kiln	Pottery, Baked clay	15/60
DQ9	Late Chunqiu Dynasty	513 ± 37 BCE	30.63	120.01	Kiln	Pottery, Baked clay	15/75
DQ10	Shang Dynasty	1300 ± 300 BCE	30.72	120.05	Kiln	Pottery, Baked clay	20/80
DQ11	Shang Dynasty	1300 ± 300 BCE	30.72	120.05	Kiln	Pottery, Baked clay	15/60
Quyang, Hebei							
DY1	Middle-Late Tang Dynasty	835 ± 72 CE	38.80	114.70	Kiln	Porcelain	2/17
DY4	Yuan Dynasty	1320 ± 49 CE	38.80	114.70	Kiln	Porcelain	1/10
DY9	Middle-Late Beisong Dynasty	1085 ± 42 CE	38.80	114.70	Kiln	Porcelain	1/6
DY15	Yuan Dynasty	1320 ± 49 CE	38.80	114.70	Kiln	Porcelain	1/8
DY16	Middle-Late Beisong Dynasty	1085 ± 42 CE	38.80	114.70	Kiln	Porcelain	1/8
DY23	Middle-Late Beisong Dynasty	1085 ± 42 CE	38.80	114.70	Kiln	Porcelain	1/6
DY30	Early Beisong Dynasty	1002 ± 42 CE	38.80	114.70	Kiln	Furnace brick	1/6
DY35	Jin Dynasty	1175 ± 60 CE	38.80	114.70	Kiln	Porcelain	2/10
DY37	Jin Dynasty	1175 ± 60 CE	38.80	114.70	Kiln	Baked clay	2/12
DY40	Middle-Late Beisong Dynasty	1085 ± 42 CE	38.80	114.70	Kiln	Porcelain	1/6
DY41	Middle-Late Beisong-Jin Dynasty	1139 ± 96 CE	38.80	114.70	Kiln	Porcelain	2/11

3. Experimental techniques

3.1. Rock magnetism

Rock magnetic experiments are designed to characterize the rock magnetic properties such as mineralogy and domain state of the samples. Some of the hysteresis loops were measured with the MicroMag 2900 AGM in the paleomagnetism laboratory at Scripps Institution of Oceanography (SIO), CA, USA and the others were measured on the MicroMag 3900 VSM in the Paleomagnetism and Geochronology Laboratory (PGL) at Institute of Geology and Geophysics, Chinese Academy of Sciences, Beijing, China. Measurements of First Order Reversal Curves (FORCs) (Roberts et al., 2000) were conducted on the same MicroMag 3900 VSM in PGL. For the purpose of determining Curie temperature (T_c) and detecting possible alteration during heating, variability of magnetization versus temperature was measured with the MMVFTB (Magnetic Measurements Variable Field Translation Balance) fixed with an oven in PGL. Rock magnetic samples analyzed at SIO are small chips while the ones used in PGL are powders.

3.2. Paleointensity

3.2.1. 'Coe–Thellier' and 'IZZI' method

A total of 918 specimens were processed for paleointensity experiments with a minimum of 4 specimens per sample. Of these, 258 were cut into cubes (1.7 cm × 1.7 cm × arbitrary height) and fixed in cubic ceramic boxes (2 cm × 2 cm × 2 cm) with fire-resistant fiber cotton. The magnetic moment of the ceramic cubes is comparable to the background of the magnetometer used for the measurements. The procedure for the paleointensity experiment followed the modified version of Thellier–Thellier method (Thellier and Thellier, 1959) by Coe (1967), referred to here as the 'Coe–Thellier' protocol. The pTRM checks were inserted at every other temperature step (Coe et al., 1978). A paleointensity furnace with temperature reproducibility within 2 °C was used for heating the specimens. Argon gas was circulated and charcoal powder was used during the heating-cooling cycle in order to reduce chemical alterations as much as possible. Heating steps were carried out from 100 °C to 580 °C with temperature intervals varying from 50 °C until 250 °C to 30 °C until 580 °C. Specimens cool in the oven after each heating step without the aid of fans, a process that takes up to ∼12 h. The laboratory field of 30 μT is applied along $-z$ axis of the specimens with a precision of 0.1 μT. The remanence was measured with the 2G 760 SQUID magnetometer. The whole procedure of the experiment was conducted in a shielded room with residual field lower than 300 nT.

The remaining 660 specimens were processed at SIO. Samples were broken into irregular chips and fixed in 12-mm diameter glass tubes with glass microfiber paper and potassium-silicate glue (KASIL). The 'IZZI' protocol was used for the paleoin-

Fig. 2. Various samples analyzed in this study: (a) baked clay from Shandong, (b) slag from Zhejiang, (c) porcelain fragment from Hebei, (d–h) pottery fragments with different shapes and decorations from Zhejiang.

tensity experiment (Tauxe and Staudigel, 2004), which is believed to be better than the traditional protocols (Aitken et al., 1988; Coe, 1967) because it can easily detect the effect of high temperature pTRM tails (Yu and Tauxe, 2005; Yu et al., 2004). The pTRM checks were also included at every other step. Specimens were heated in one of two ovens, which have residual fields less than 10 nT during zero-field steps, in the paleomagnetic shielded room at SIO. Measurements were made on a 2G cryogenic magnetometer. Heating steps were carried out from 100 °C to 580 °C (with a few up to 600 °C) with temperature intervals varying from 100 °C to 15 °C, generally larger for low temperatures and smaller for high temperatures. Specimens were cooled in the oven after each heating step with a fan and cooling times are 30–45 minutes. A laboratory field is applied along $-z$ axis of the specimens and field value of 30 μT or 50 μT was chosen depending on the expected ancient field of samples.

3.2.2. Anisotropy correction

The effect of anisotropy of TRM (ATRM) on paleointensity estimation has long been recognized (Aitken et al., 1981, 1988; Rogers et al., 1979). TRM anisotropy is sometimes observed in geological samples, but occurs frequently in archaeological artifacts because of manufacturing procedures, which makes the anisotropy correction in archaeological study non-trivial. The bias in paleointensity caused by ATRM can be corrected by determining the anisotropy tensor of each specimen (Selkin et al., 2000; Veitch et al., 1984). This can be determined by anisotropy of magnetic susceptibility (AMS) or anisotropy of anhysteretic remanent magnetization (AARM) or ATRM. While it is generally agreed that AMS is a poor approximation for ATRM, the preference for AARM and ATRM remains controversial. Some authors prefer the ATRM correction because in theory AARM is different from ATRM (Chauvin et al., 2000). Others argue that AARM is preferable because the corrections are usually similar (Ben-Yosef et al., 2008a; Mitra et al., 2013), it is faster to determine the AARM tensor than the ATRM one, and there is no further laboratory alteration with the AARM tensor. Some studies use a partial TRM (pTRM) to determine the ATRM tensor in order to avoid bias introduced by alteration when heating to high temperatures (Chauvin et al., 2000; Genevey and Gallet, 2002; Hill et al., 2008), while total TRMs are used in other studies based on the assumption that total TRM correction avoids the complications of pTRM tails that may affect pTRMs. The use of pTRM checks insures that the ATRM tensor has not been affected by alteration (Shaar et al., 2010, 2011).

Here we impart a total TRM along the six axes of each specimen ($\pm x$, $\pm y$, $\pm z$) following the method of Veitch et al. (1984). For some specimens we used an initial demagnetization step to determine a baseline. When calculating the ATRM tensor, we prefer the original method proposed by Veitch et al. (1984) to the modified version by Selkin et al. (2000) because the latter might change paleointensity parameters which are critical to data selection (Paterson, 2013). Following the six ATRM measurements, we include an additional step, which is a repeat of the first measurement position to test for possible alteration during the heatings required to measure the tensor.

3.2.3. Cooling rate correction

Dodson and McClelland-Brown (1980) showed that blocking temperatures of single domain grains are related to the cooling rate and the TRM acquired at different cooling rates in the same field might differ significantly. This will bias the estimation of paleointensity (Halgedahl et al., 1980). In order to obtain the most

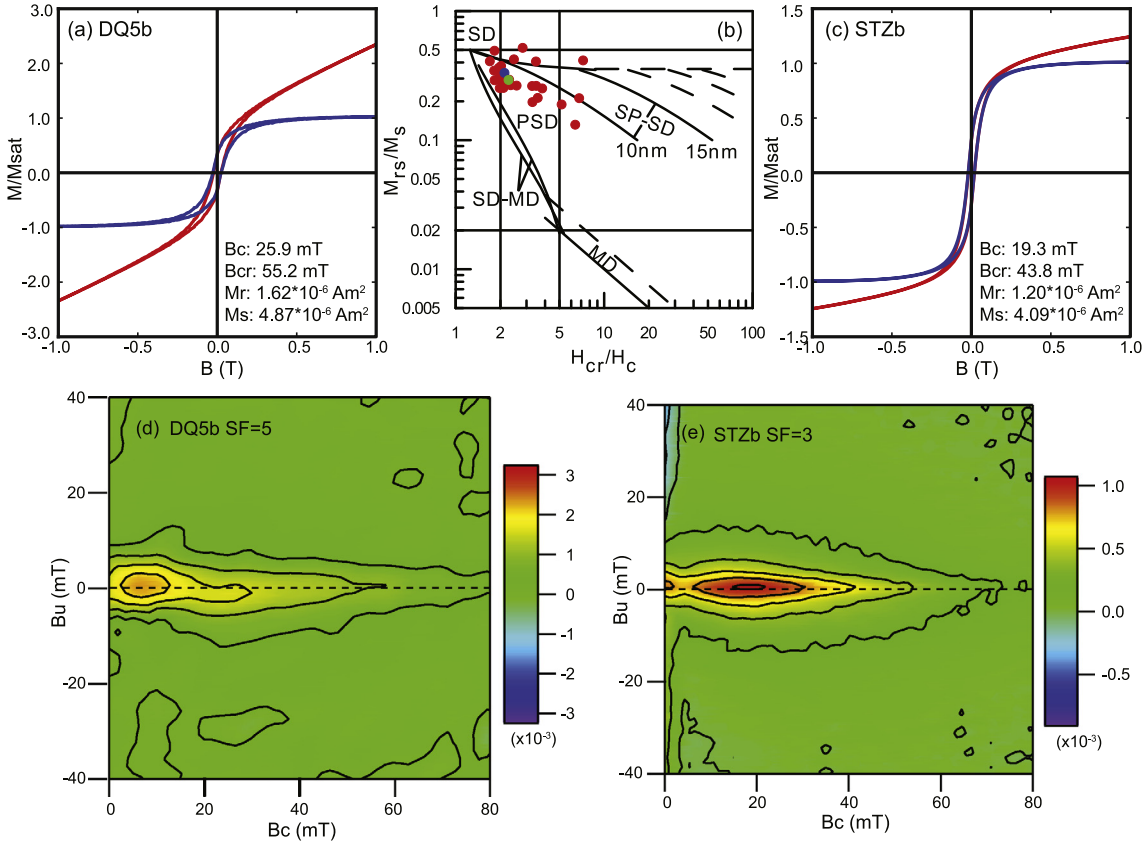

Fig. 3. (a) and (c) Hysteresis loops of representative samples. Red (blue) loop is before (after) paramagnetic correction. The hysteretic parameters, B_c: coercivity, B_{cr}: remanence coercivity, M_r: remanent magnetization and M_s: saturated magnetization, are listed on the plots. Data are analyzed with the software of Pmagpy-2.184 by Lisa Tauxe. (b) Day plot after Dunlop (2002a, 2002b). Red dots are projections of hysteretic parameters. Samples of DQ5b and STZb are marked as blue and green dots separately. (d) and (e) FORC plots after Roberts et al. (2000). Data are analyzed with the software of FORCinel_1.17. (For interpretation of the references to color in this figure legend, the reader is referred to the web version of this article.)

accurate results, we applied a cooling rate correction for each specimen after the paleointensity experiment. We followed the procedure suggested by Genevey and Gallet (2002) and used the same temperature as for the ATRM correction (the total TRM). We used a three-step protocol (4 in some cases including the baseline step). First, specimens were cooled 'fast', in about 30 minutes, to acquire TRM_1. Then they were cooled in a 'slow' step (without a fan) which takes ~12 h to cool to 40 °C from 580 °C for TRM_2. Finally, they were subjected to a second 'fast' step similar to the first for TRM_3. The third step is for monitoring of alterations. The correction factor was calculated from the ratio of the average of TRM_1 and TRM_3 to TRM_2. For consistency, the same specimens were used for all procedures during the paleointensity experiment, ATRM correction and cooling rate correction.

The cooling rate correction was only applied for specimens processed at SIO because ovens there were cooled with a fan. The furnace used in PGL does not have a fan and specimens are cooled naturally, taking ~12 h cooling to room temperature from 600 °C. Therefore a cooling rate correction is not necessary for specimens processed in PGL, assuming that the original cooling also took of the order of 12 h.

4. Results

4.1. Rock magnetic results

For the purpose of detecting the magnetic phases, representative sister specimens were selected for the hysteresis loops and FORC measurements. Most of the specimens show similar hysteresis behavior (Figs. 3a, c) with slightly wasp-waisted or goose-necked shapes indicating either SP/SD mixtures or mixtures of different magnetic phases (Tauxe et al., 1996). Samples are generally saturated before 300 mT and the coercivity (B_c) ranges from ~10 mT to ~35 mT, which show the dominance of soft magnetic minerals. The hysteresis parameters are calculated following Tauxe et al. (2010) and projected on the Day plot (Day et al., 1977) extended by Dunlop (2002a, 2002b). Most of the specimens fall into the pseudo-single domain (PSD) area and close to single domain (SD) region (Fig. 3b), which allows us to infer that SD particles mixed with superparamagnetic (SP) grains are dominant. This is supported by the FORC plots (Figs. 3d, e), which show weak-interaction SD particles mixed with SP grains (Roberts et al., 2000). The fine-grained composition of samples assures their possibility for achieving accurate paleointensity values.

The variations of magnetization versus temperature (M–T) are measured for determination of Curie temperature (T_c) and detection of possible alteration during heating. T_cs estimated from M–T curves range from ~550 °C to ~580 °C, indicating Ti-poor titanomagnetite or magnetite as the main magnetic mineral. This is in agreement with the hysteresis analysis, which shows a dominant low coercivity component (Dunlop and Özdemir, 1997). Representative curves (Fig. 4) are reasonably reversible indicating slight or no alteration during heating, a prerequisite for successful paleointensity experiments.

4.2. Paleointensity results

The selection parameters during paleointensity data analysis are crucial to the reliability of intensity estimation. Selection criteria used in this study are listed in Table S2. The upper bound for

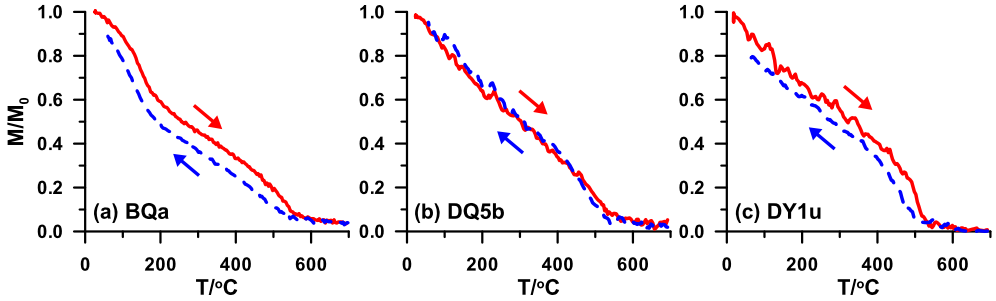

Fig. 4. Normalized magnetization variations versus temperatures of representative samples. Samples are cooked in air in an applied field of ~1 T with heating/cooling rates of 30 °C/min. Red solid (blue dashed) line represents heating (cooling) procedure. (For interpretation of the references to color in this figure legend, the reader is referred to the web version of this article.)

the scatter parameter, β (Tauxe and Staudigel, 2004) determined by the standard error of slope of the best fit line normalized to the absolute value of slope is set as 0.09. The upper bound for DANG, the deviation angle between the best fit line and the line determined by the center of mass and the origin, is constrained to be 7.5° (Tauxe and Staudigel, 2004). The maximum angle of deviation (MAD) describing the scatter of NRM points about the best fit line is limited to be 10° (Kirschvink, 1980). DRAT and DRATS are two important parameters representing the quality of pTRM checks, which are affected by measurement noise or alteration. DRAT is the maximum difference between pTRM and the pTRM check at a given temperature step normalized by the length of the best fit line (Selkin et al., 2000) while DRATs is the difference sum between pTRM and relative pTRM check normalized by the pTRM acquired by cooling from maximum temperature of the best fit line to room temperature (Kissel and Laj, 2004; Tauxe and Staudigel, 2004). Both are limited to be 10% here. The remanence fraction f is calculated by the NRM component of the best fit line on the Arai plot (Nagata et al., 1963) over the intercept of the best fit line on NRM axis and we limit it to 0.54 (Coe et al., 1978). f_{vds} is an improved version of f calculated by the ratio of NRM component of the best fit line to the vector difference sum of the entire NRM (Tauxe and Staudigel, 2004) and is constrained to 0.6. The maximum extent of alteration during TRM anisotropy correction (alter_atrm) is set to be 6% and that during cooling rate correction (alter_cool) is 5%. For the sample level, at least two accepted specimens should be included when calculate the average intensity and the standard deviation of mean intensity (σ) should be either less than 10% or smaller than 5 μT.

A total of 457 out of 918 specimens pass the selection criteria, for a success rate of ~50%. However, the success rate varies among the four studied locations, which is ~30% (80/264) in Shandong, ~73% (11/15) in Liaoning, ~63% (287/452) in Zhejiang and 42% (79/187) in Hebei. The representative accepted specimens are shown in Fig. 5a–c; these typically have one component trending to the origin (Figs. 5a, b) or a negligible soft component (Fig. 5c) removed by 150 °C evident in the orthogonal projection plots and show straight-line behavior on the Arai plots. Specimens are rejected for three reasons generally: alteration during the experiment leads to failure of the pTRM check (Fig. 5d), curved behavior caused by MD particles (Dunlop and Xu, 1994; Xu and Dunlop, 1994) (Fig. 5e, many rejected specimens from Shandong are in this case) and large secondary components which overprint the original remanence (Fig. 5f) and lead to multiple slopes in the Arai plots. The accepted samples (91 in total) are listed in Table 2 and the specimen level results are listed in Table S3. Data are analyzed with PmagPy software by Lisa Tauxe including the Thellier GUI program by Shaar and Tauxe (2013).

The anisotropy of the studied specimens is not so strong as expected for archaeomagnetic materials, with τ_1/τ_3 varying between 1.02 ~ 1.85 (97% of them less than 1.5), where τ_1 and τ_3 are the maximum and minimum eigenvalues of the ATRM tensors respectively (Tauxe et al., 2010). The alterations during the TRM anisotropy correction experiment are generally less than 10% (Fig. S2a) and we exclude those with more than 6% to make sure accurate anisotropic tensors are calculated. The extent of correction described by the ratio of the intensity value after ATRM correction (B_{ac}) to the raw intensity before any correction (B_{raw}) ranges from 0.7 to 1.3 (but is generally between 0.9 ~ 1.1, Fig. S2b). The standard deviations (σ) before and after ATRM correction are compared and 70% of them become smaller after the correction (Fig. S3) indicating the effectiveness of the anisotropy correction. Most of the alterations during cooling rate correction are less than 5% (Fig. S2c) and the ones exceeding 5% are rejected. The correction factors are between 0.85 ~ 1.05 (Fig. S2d).

5. Discussion

The important location and abundant archaeological artifacts make archaeomagnetic study in China both necessary and achievable. In this paper, a number of reliable archaeointensity results from four different locations are reported. The reliability of these data is assured by the use of a robust experiment procedure and stringent selection criteria. The dominant fine-grained titanomagnetite or magnetite minerals and their stability during heating indicate their suitability for paleointensity experiments. Most of the studied samples behave very well during the paleointensity experiment and a high average success rate of ~50% is obtained. However, the problem of age control remains. Any kind of material suitable for radiocarbon dating, such as charcoal, is unavailable. Therefore all the ages of the samples are estimated from the archaeological context. Nonetheless, these have great utility for two reasons. One is the extensive historical record in China makes the characteristic of artifacts during each period quite diagnostic. For example, the workmanship and decoration of potteries evolve with time, allowing experienced archaeologists to recognize them with great accuracy. The other reason is internal consistency of data thought to have the same age.

In order to detect the regional variations of the geomagnetic field in Eastern Asia, we compare our new results with the published data from China and Japan compiled in the GEOMAGIA50 database (Donadini et al., 2006; Korhonen et al., 2008) (Fig. 6). The experimental details of the published data are generally not well documented and may be of uneven quality. At present, the database only allows us to select based on the general method, the number of specimens and the internal consistency of the average. Therefore, we choose only those data obtained through the double-heating protocol (widely considered the most robust), those were based on averages of at least two specimens with a standard deviation of mean intensity less than 10% or 5 μT. The site locations of the selected data are shown in Fig. 1.

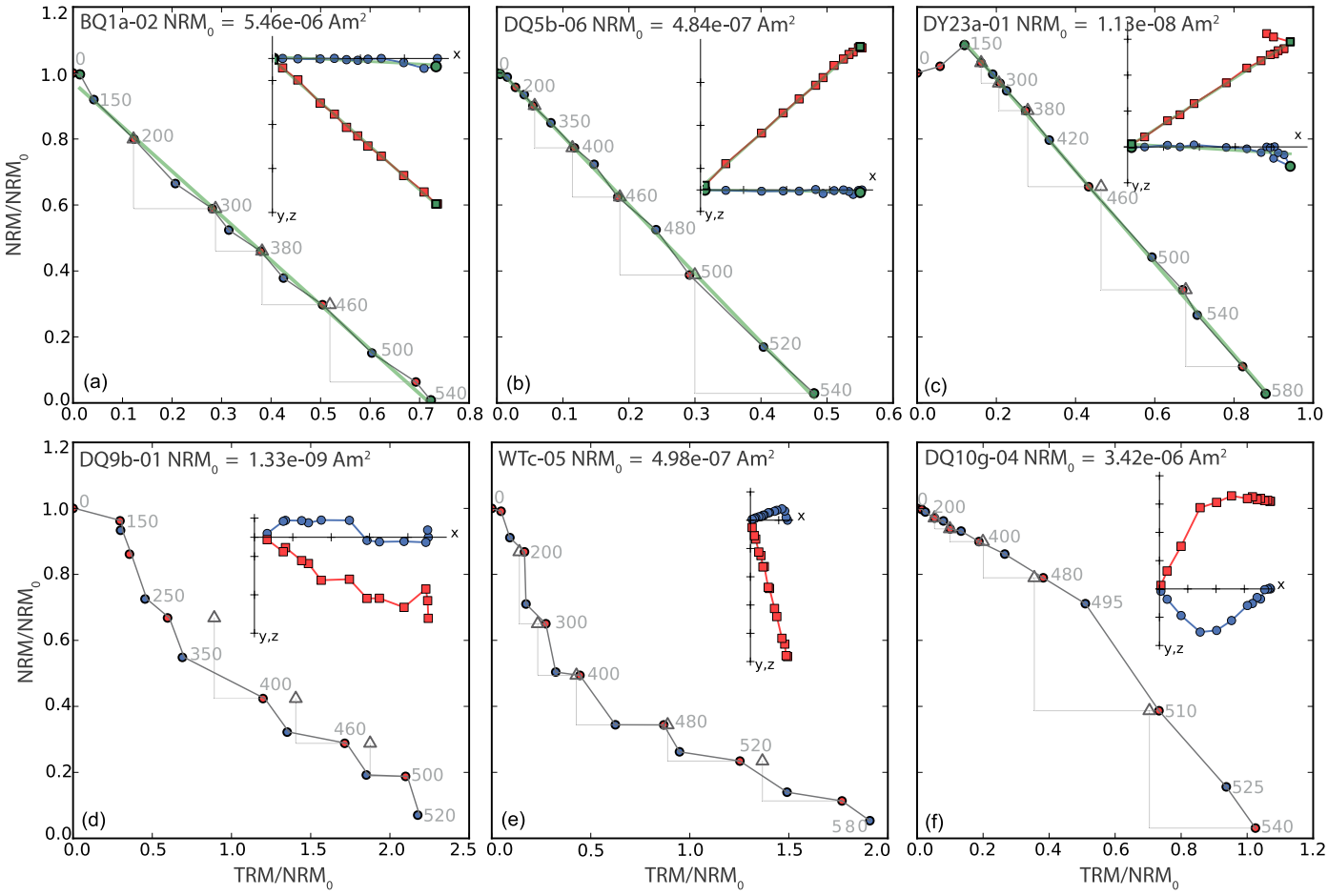

Fig. 5. Arai plots and orthogonal projections (insets) of representative accepted (a, b, c) and rejected (d, e, f) specimens. Numbers on the plot are temperature steps in centigrade (°C). Red squares (blue solid circles) are projections on the vertical (horizontal) plane. The 'x' axis is rotated to NRM direction. (For interpretation of the references to color in this figure legend, the reader is referred to the web version of this article.)

We try to explore the possible global behavior of the geomagnetic field during the past 8 kyr by comparing the VADM variations in Eastern Asia (100°E–140°E) with those in the Middle East (30°E–70°E) and Southern Europe (10°W–30°E) (Fig. 7), where a number of archaeomagnetic studies were conducted. Because most of the data from Eastern Asia are concentrated between 25°N–45°N, we use data from the same latitude band in the Middle East and Europe to avoid the influence of latitudinal gradients (Mitra et al., 2013). The same data selection criteria used in Fig. 6 is adopted here. Besides that, some new published data that were not previously in the database are included: data from Yu (2012) in Japan (Fig. 7a), data from Shaar et al. (2011) and Ertepinar et al. (2012) in the Middle East (Fig. 7b) and data from Gómez-Paccard et al. (2012) and Tema et al. (2012) in Europe (Fig. 7c). The locations map of data points used in this study are shown in Fig. S4.

5.1. New paleointensity low

One surprising feature of the data shown in Fig. 6 is the appearance of a period of extremely low paleointensity ($\sim 2 \times 10^{22}$ Am^2) at ~2250 BCE. The observed values (shown in red in Fig. S5) are lower than any of the published data for the period 5000–2000 BCE (blue in Fig. S5). One possible interpretation is that these represent a hitherto undetected geomagnetic excursion. However, since the definition of geomagnetic excursion is generally based on direction (Cox et al., 1975; Vandamme, 1994) and we have results from only two samples here, further evidence is necessary. We will refer to it as a 'Decrease in Paleointensity' (DIP) following the usage of Kent and Schneider (1995).

5.2. Rapid change in field intensity

Our new data show a six-fold increase from ~2250 BCE to ~1300 BCE with VADM values rising sharply from $\sim 2 \times 10^{22}$ to $\sim 13 \times 10^{22}$ Am^2. The rate of change of geomagnetic intensity during this period is ~6 μT/century or 47% per century (calculated from the lowest value at ~2250 BCE and highest value at ~1300 BCE). This variation is consistent with the upper bounds of ~0.62 μT/yr suggested by Livermore et al. (2014) but not as fast as the one reported by Gómez-Paccard et al. (2012) with a rate that varies from ~12 to ~80 μT/century between 600–1300 CE in western Europe and much lower than the one reported by Shaar et al. (2011) in which the intensity changes ~30 μT in 30 yrs (910–890 BCE) in Levantine area. But a six-fold change of the field (2×10^{22}–13×10^{22} Am^2) in less than 1000 yrs is still abrupt. One thing that should be mentioned is that the data from ~1300 BCE, ~513 BCE and ~348 BCE from sites DQ7–DQ11 seem to be quite scattered with respect to the trend of VADM versus time. But if we calculate the average value of all acceptable samples from each site, consistent mean intensities (with $\sigma < 10\%$) can be obtained except σ of DQ7 is 10.4% (Table S4). However, we argue that the scatter in the data is genuine geomagnetic field behavior and not experimental noise. Hence, we prefer to treat the sample results to avoid averaging out fluctuations of the geomagnetic field. For example, the variations of field intensity shown

Table 2
The list of accepted results on sample level. B_{lab}: applied field in the lab; B_{acc}: average paleointensity of a sample after anisotropy and cooling rate correction (those without cooling rate correction are marked with '*'); σ_B: standard deviation of B_{acc}; σ_{VADM}: standard deviation of VADM; n_a: number of specimens accepted.

Sample	B_{lab} (μT)	B_{acc} (μT)	σ_B (μT)	σ_B (%)	VADM ($\times 10^{22}$ Am^2)	σ_{VADM} ($\times 10^{22}$ Am^2)	n_a	Method
BQa	30	35.7	2.0	5.6	6.41	0.36	5	IZZI
BQb	30	33.0*	1.1	3.3	5.93	0.2	8	Coe–Thellier
DZJa	30	30.8*	2.3	7.3	5.46	0.4	6	Coe–Thellier
DZJe	30	34.7	2.0	5.7	6.17	0.35	3	IZZI
GDDc	30	26.1	4.5	17.3	4.66	0.8	3	IZZI
GDDd	30	31.1	2.1	6.7	5.55	0.37	3	IZZI
GJCa	30	25.4	2.8	10.9	4.45	0.49	5	IZZI
LCZa	30	16.8*	2.0	12.1	3.06	0.37	2	Coe–Thellier
LCZc	30	24.7	1.8	7.2	4.5	0.32	6	IZZI
QJZa	30	36.5*	1.9	5.1	6.5	0.33	3	Coe–Thellier
QJZd	30	36.4	2.3	6.3	6.49	0.41	5	IZZI
SWC4a	30	46.9*	2.6	5.4	8.38	0.46	6	Coe–Thellier
SWC4b	30	44.0*	1.5	3.4	7.86	0.27	3	Coe–Thellier
SWC5b	30	58.0*	3.3	5.6	10.37	0.58	7	Coe–Thellier
XJTc	30	29.9	1.6	5.5	5.33	0.29	4	IZZI
YJC1a	30	51.5	2.1	4	9.01	0.36	6	IZZI
ZJZa	30	12.8*	1.4	10.9	2.3	0.25	8	Coe–Thellier
ZJZd	30	29.2	0.9	2.9	5.21	0.15	4	IZZI
ZJZf	30	25.9	3.8	14.8	4.63	0.68	4	IZZI
DQ1a	30	47.7	1.4	2.9	9.24	0.26	4	IZZI
DQ1c	30	41.1	1.5	3.6	7.98	0.29	4	IZZI
DQ2a	30	52.2	3.1	6	10.13	0.61	3	IZZI
DQ3a	30	58.8	5.8	9.8	11.41	1.12	6	IZZI
DQ4a	30	41.7	0.8	1.9	8.09	0.15	5	IZZI
DQ4c	30	41.6	0.7	1.8	8.07	0.14	4	IZZI
DQ5a	30	59.9	1.9	3.1	11.66	0.36	5	IZZI
DQ5b	30	61.1	3.2	5.2	11.89	0.62	8	IZZI
DQ6b	30	60.1	3.9	6.5	11.7	0.76	4	IZZI
DQ7a	50	35.0	0.7	2	6.79	0.14	4	IZZI
DQ7e	50	37.4	0.4	1	7.25	0.07	3	IZZI
DQ7f	50	42.7	1.7	4	8.28	0.33	4	IZZI
DQ7g	50	44.3	1.2	2.6	8.59	0.22	4	IZZI
DQ7h	50	40.3	2.4	6	7.82	0.47	4	IZZI
DQ7j	50	49.6	2.9	5.8	9.61	0.56	3	IZZI
DQ7k	50	48.1	3.6	7.5	9.32	0.7	4	IZZI
DQ7l	50	41.7	2.0	4.8	8.09	0.39	4	IZZI
DQ7o	50	46.7	1.7	3.6	9.05	0.33	4	IZZI
DQ7p	50	45.8	0.7	1.5	8.88	0.14	4	IZZI
DQ7q	50	48.0	0.5	0.9	9.32	0.09	3	IZZI
DQ7r	50	40.8	0.5	1.3	7.9	0.1	4	IZZI
DQ8a	50	51.9	1.1	2.2	10.07	0.22	3	IZZI
DQ8b	50	49.5	3.4	6.9	9.6	0.67	3	IZZI
DQ8d	50	45.7	1.6	3.6	8.86	0.32	3	IZZI
DQ8f	50	39.0	0.2	0.6	7.57	0.05	4	IZZI
DQ8g	50	48.4	1.5	3	9.39	0.28	4	IZZI
DQ8h	50	50.9	1.6	3.2	9.88	0.31	3	IZZI
DQ8i	50	53.6	1.1	2	10.39	0.2	4	IZZI
DQ8j	50	50.1	2.8	5.5	9.72	0.54	4	IZZI
DQ8k	50	49.7	2.4	4.9	9.65	0.47	4	IZZI
DQ8m	50	45.3	1.3	2.9	8.78	0.25	4	IZZI
DQ8p	50	46.8	2.0	4.4	9.07	0.39	3	IZZI
DQ9a	30	47.7	1.4	3	9.24	0.27	5	IZZI
DQ9d	30	50.8	2.9	5.6	9.84	0.56	5	IZZI
DQ9e	30	48.0	1.8	3.7	9.31	0.35	4	IZZI
DQ9f	30	45.3	1.5	3.4	8.78	0.3	5	IZZI
DQ9h	30	47.5	2.8	6	9.22	0.55	5	IZZI
DQ9i	30	43.9	3.2	7.3	8.51	0.62	4	IZZI
DQ9l	30	46.2	0.7	1.5	8.96	0.14	3	IZZI
DQ9m	30	50.4	1.6	3.2	9.77	0.32	5	IZZI
DQ9o	30	55.5	4.9	8.9	10.76	0.96	4	IZZI
DQ9p	30	57.6	1.5	2.5	11.16	0.28	3	IZZI
DQ10b	50	60.3	1.6	2.6	11.68	0.3	4	IZZI
DQ10e	50	66.8	4.8	7.1	12.94	0.92	4	IZZI
DQ10f	50	56.9	4.0	7	11.01	0.77	3	IZZI
DQ10h	50	66.6	4.3	6.5	12.9	0.84	4	IZZI
DQ10j	50	53.2	1.6	3	10.31	0.31	4	IZZI
DQ10q	50	63.4	3.0	4.7	12.28	0.58	4	IZZI
DQ10r	50	60.7	3.8	6.2	11.75	0.73	4	IZZI
DQ10s	50	65.1	4.9	7.5	12.62	0.95	4	IZZI
DQ11a	50	54.7	2.1	3.8	10.59	0.41	3	IZZI
DQ11c	50	57.3	4.8	8.3	11.09	0.92	4	IZZI
DQ11d	50	50.5	2.9	5.7	9.79	0.56	4	IZZI
DQ11e	50	64.3	1.8	2.9	12.45	0.36	4	IZZI

Table 2 (*continued*)

Sample	B_{lab} (μT)	B_{acc} (μT)	σ_B (μT)	σ_B (%)	VADM ($\times 10^{22}$ Am^2)	σ_{VADM} ($\times 10^{22}$ Am^2)	n_a	Method
DQ11f	50	52.8	3.2	6	10.23	0.62	4	IZZI
DQ11g	50	61.6	6.1	9.9	11.93	1.18	5	IZZI
DQ11l	50	54.1	1.8	3.3	10.48	0.34	4	IZZI
DQ11m	50	54.2	4.1	7.5	10.49	0.79	3	IZZI
DQ11n	50	59.3	0.9	1.5	11.48	0.18	3	IZZI
DQ11p	50	59.6	3.4	5.6	11.55	0.65	3	IZZI
DY15	30	55.6*	2.1	3.8	9.75	0.37	8	Coe–Thellier
DY16	30	58.9*	2.1	3.5	10.32	0.36	4	Coe–Thellier
DY1a	30	58.0*	2.6	4.4	10.16	0.45	9	Coe–Thellier
DY1u	30	64.6	3.1	4.8	11.33	0.54	5	IZZI
DY23a	30	43.4	1.4	3.3	7.6	0.25	5	IZZI
DY30a	30	57.2	1.4	2.5	10.02	0.25	6	IZZI
DY35a	30	51.9*	0.5	0.9	9.1	0.08	5	Coe–Thellier
DY35u	30	52.6	1.8	3.4	9.21	0.31	4	IZZI
DY37a	30	49.3	0.7	1.5	8.63	0.13	4	Coe–Thellier
DY37u	30	46.7	2.5	5.4	8.18	0.44	6	IZZI
DY40a	30	55.1	1.7	3	9.65	0.29	4	IZZI
DY41c	30	52.9	1.4	2.6	9.28	0.24	5	Coe–Thellier
DY4a	30	46.7	3.7	8	8.18	0.65	8	Coe–Thellier
DY9a	30	51.6	1.4	2.8	9.04	0.25	6	IZZI

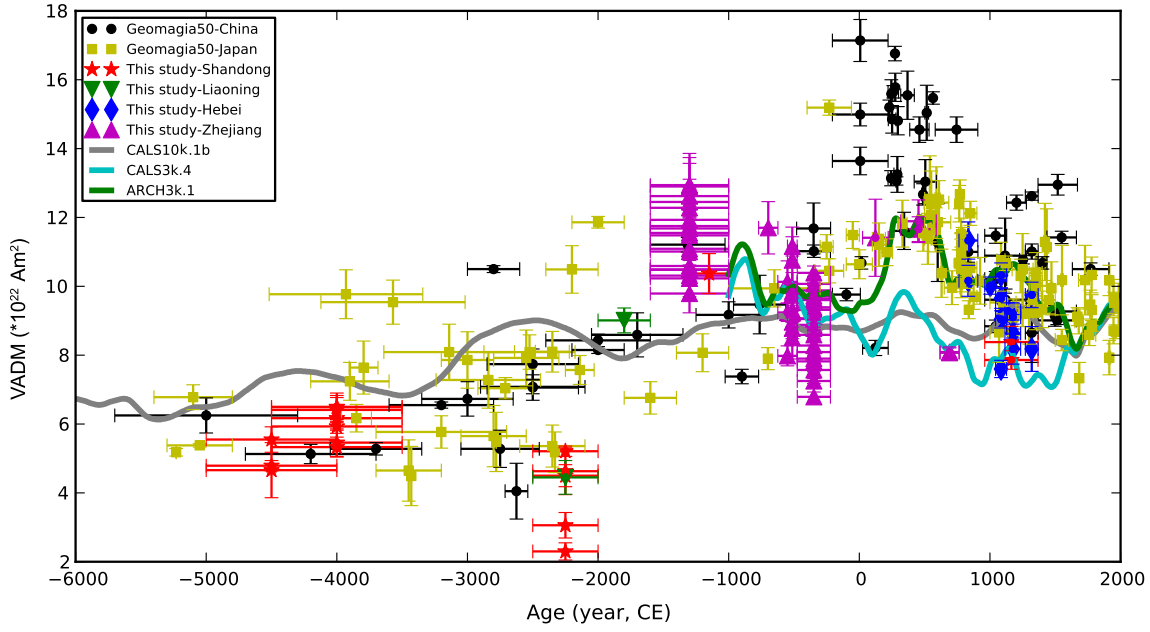

Fig. 6. Regional model of virtual axial dipole moments (VADMs) in Eastern Asia. Black solid circles/yellow squares are the accepted published data in China/Japan from GEOMAGIA50 database. Data selection criteria please see the text. Red stars/green triangles down/magenta triangles/blue diamonds represent new data of this study from Shandong/Liaoning/Zhejiang/Hebei location. The color lines are predictions from global models of CALS10k.1b (gray), CALS3k.4 (cyan) and ARCH3k.1 (green) at the center of China (35°N, 105°E). (For interpretation of the references to color in this figure legend, the reader is referred to the web version of this article.)

by our new results during the three period of 1600–1000 BCE, 550–476 BCE and 475–221 BCE are $\sim 10 \times 10^{22}$–13×10^{22} Am^2 ($\sim$2 μT/century), $\sim 9 \times 10^{22}$–11×10^{22} Am^2 ($\sim$19 μT/century) and $\sim 7 \times 10^{22}$–10×10^{22} Am^2 ($\sim$7 μT/century) respectively.

5.3. A possible spike at ~200 CE

Ben-Yosef et al. (2009) used the term 'geomagnetic spike' to refer to a short-lived peak in the geomagnetic field, in contrast to 'excursion' or 'DIP' reserved for periods of unusually low geomagnetic field intensities. There is no formal definition for a 'geomagnetic spike' presently. Here, we suggest using a definition of a sharp increase in the field intensity to more than twice the present value ($\sim 16 \times 10^{22}$ Am^2 in less than 500 yrs as a 'spike'. Such a spike was suggested at ~200 CE in the published data from Wei et al. (1982, 1986). This feature, although based on data without modern precautions against the effects of laboratory alteration or unremoved pTRM tails, is supported by a great number of data from different places (including a data point from Japan). However, we failed to confirm the existence of the intensity spike in results reported here. Therefore, additional evidence is required to establish the validity of the 200 CE 'spike'.

5.4. Comparison with the predictions from global models

When comparing our data with the predictions of the variation of geomagnetic field at the center of China (35°N, 105°E) from the three global models, our new data fit well with the ARCH3k.1 model (Korte et al., 2009) but deviate significantly at certain periods from the CALS3k.4 (Korte and Constable, 2011) and CALS10k.1b model (Korte et al., 2011) (Fig. 6). This is likely to be because of the different input data of the models. The models including the sedimentary data are greatly smoothed, especially for the CALS10k.1b

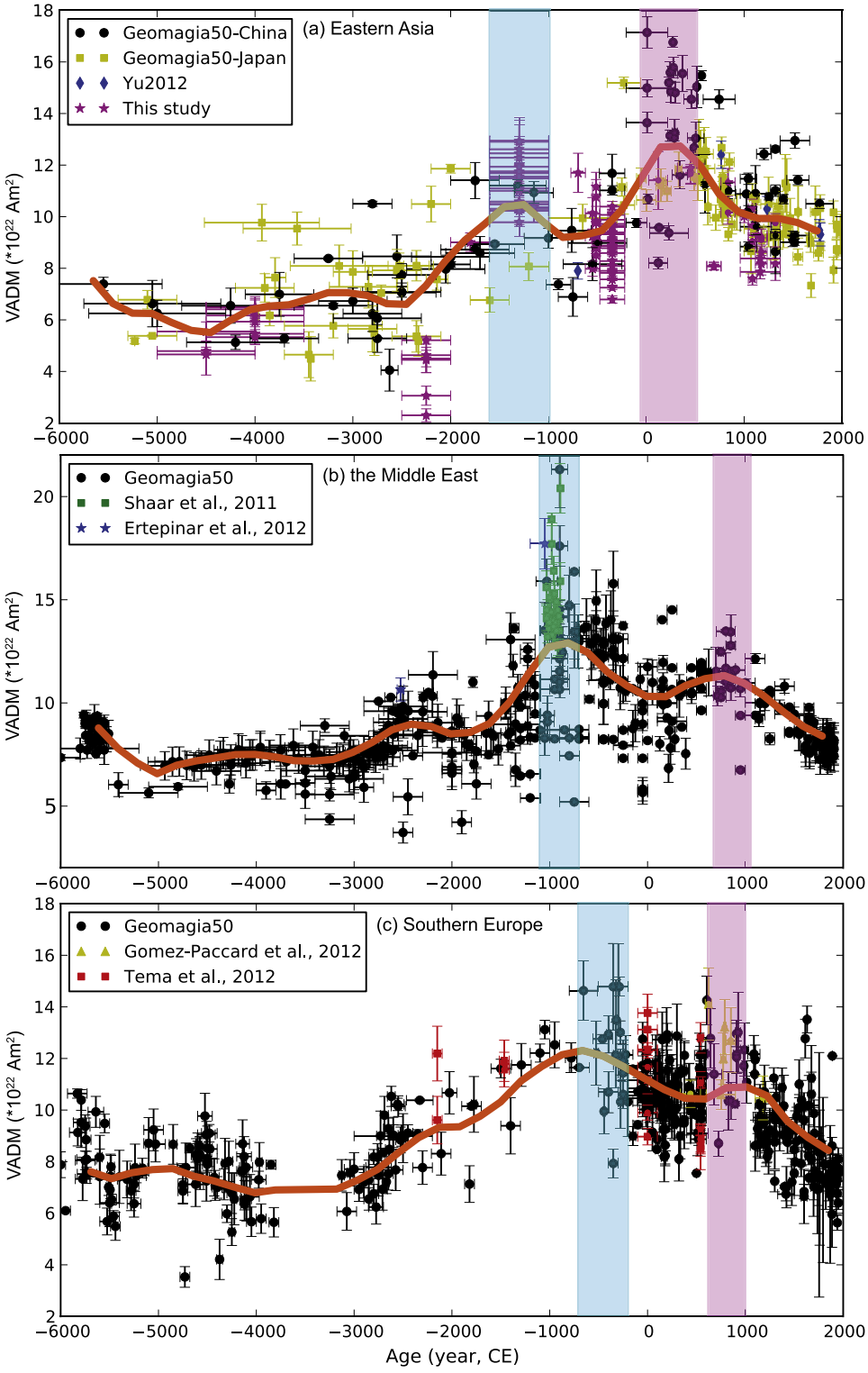

Fig. 7. Comparison of VADM variations among areas of (a) Eastern Asia, (b) the Middle East and (c) Southern Europe. Data symbols please check the legend in each plot. Data selection criteria please see the text. Peaks of each area are highlighted by cyan and pink shades. The orange lines are variations of average VADMs calculated every 400 yrs with a 200-yrs sliding window. (For interpretation of the references to color in this figure legend, the reader is referred to the web version of this article.)

model. An implication here is that more reliable input data are necessary to improve the global models.

5.5. Improvement of regional model of Eastern Asia

Apart from the 'spike' discussed previously, the new data reported here are generally consistent with the published data from China and Japan, showing strong fluctuations of the geomagnetic field during the past 8 kyr. We provide a great number of reliable archaeointensity data for the Eastern Asia where paleointensity data are sparse and thus improve the regional model of the geomagnetic field in Eastern Asia greatly, which have potential implications for archaeomagnetic dating in this area in the future.

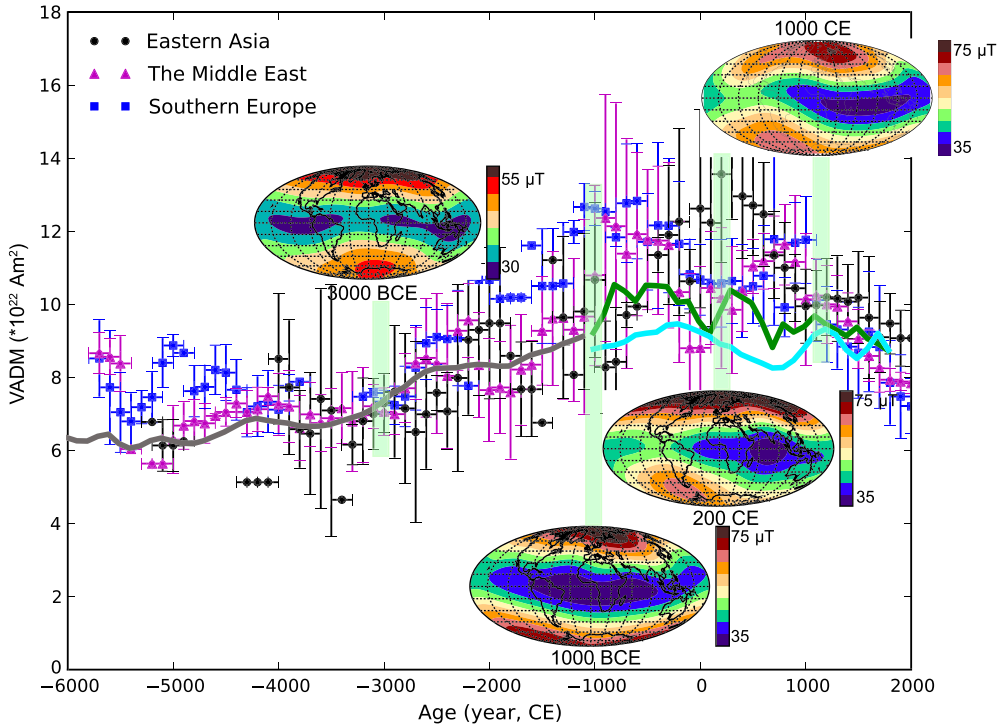

Fig. 8. Variations of average VADMs in the areas of Eastern Asia (black solid circles), the Middle East (magenta triangles) and Southern Europe (blue squares). Data selection criteria please see the text. The averages are calculated every 200 yrs with a 100-yrs sliding window. The insets are predictions of the geomagnetic field intensities at the earth surface from CALS10k.1b (older than 1000 BCE) or ARCH3k.1 (younger than 1000 BCE) model at different time periods. Maps of geomagnetic fields are generated by MAGMAP of R.L. Parker. Gray/cyan/green heavy line represents the axial dipole moment predicted by CALS10k.1b/CALS3k.4/ARCH3k.1. (For interpretation of the references to color in this figure legend, the reader is referred to the web version of this article.)

5.6. Comparison among Eastern Asia, the Middle East and Southern Europe

As most of the data in the GEOMAGIA50 database come from Eurasia, we consider now variations as a function of longitude across Eurasia. In order to eliminate latitudinal gradients, such as those documented by Mitra et al. (2013), we consider data in three longitudinal bands (Eastern Asia: 100°E–140°E, the Middle East: 30°E–70°E and Southern Europe: 10°W–30°E), with bounding latitudes of 25°N and 45°N (see Fig. S4). The general trend of intensity variation since ~8 ka is one of fairly low field strengths (VADMs: $\sim 5 \times 10^{22}$ Am^2 around 5000 BCE, rising to up to three times that, with several peaks in intensity (shown in cyan and pink bands in Fig. 7) followed by a general decline to the present field value of approximately 8×10^{22} Am^2. This general trend may be dominated by the behavior of the geomagnetic dipole (shown in Fig. 8 for various models). However, the timing and amplitude of the peaks vary in different areas.

The first peak in field intensity (indicated by cyan bands in Fig. 7) appears to have occurred at ~1300 BCE in Eastern Asia (Fig. 7a), at around 1000 BCE in the Middle East (Fig. 7b) and at ~500 BCE in Southern Europe (Fig. 7c) and was largest in the Middle East. The second peak (indicated by pink bands in Fig. 7) appears at ~200 CE in Eastern Asia (Fig. 7a), at ~800 CE in the Middle East (Fig. 7b) and around ~700 CE in Southern Europe (Fig. 7c). If these are indeed the same features, the first peak appears progressively from east to west, which could be explained by the well-known westward drift of geomagnetic field (Bullard et al., 1950; Vestine and Kahle, 1968). However, it traveled ~21 km/yr from Eastern Asia to the Middle East but only ~4 km/yr from the Middle East to Europe. The second peak traveled ~12 km/yr from Eastern Asia to the Middle East and then from west to east (from Europe to the Middle East) with a speed of ~20 km/yr. Dumberry and Finlay (2007) reported that both eastward and westward drift of geomagnetic field can occur, which might help to explain the behavior of the second peak and the extremely discordant speed of the first peak by attributing the lower speed from the Middle East to Europe to the stack of eastward and westward movement. Nevertheless the result mentioned by Dumberry and Finlay (2007) is just for the last three millennia and little robust information could be obtained for older periods because of the sparseness of the database. Therefore, we have not enough evidence for the scenario of westward drift even though it is a possibility.

An alternative view of the behavior observed in Fig. 7 is that the peaks are not traveling features of the geomagnetic field (say migrating flux patches), but are distinct features of the non-dipole field that grow and decay in place (Amit et al., 2011; Hartmann et al., 2011). To investigate this possibility, we calculate the average VADMs for Eastern Asia, the Middle East and Southern Europe using the same data set (both published and new) in Fig. 7 for each region and plot them in Fig. 8. The average VADMs of the three areas are well grouped at about ~3000 BCE and approximately equivalent to the strength of the axial dipole (heavy gray line) at that time. The values are more scattered at ~1000 BCE and 200 CE, however, and in places much stronger than the axial dipole moment (heavy cyan and green lines), indicating strong non-dipolar behavior. The divergence from the axial dipole continues through to about 1000 CE, when the local fields converge again with the axial dipole moment (heavy cyan and green lines).

Interestingly, the local agreement or disagreement of the average VADMs across Eurasia does not always agree with the patterns of intensity across the globe predicted by the models (insets to Fig. 8). The intensity of surface field at 3000 BCE predicted by the CALS10k.1b model appears to be dipolar and that at 200 CE (predicted by the ARCK3k.1) model is much more non-dipolar in character. These agree with the variation of average VADMs which are well grouped at about ~3000 BCE and scattered at ~200 CE. However, they do not agree around 1000 BCE when the average

VADMs are scattered but the surface field is predicted to be more dipolar and vice versa at 1000 CE. As shown in Fig. 6, there is rather poor agreement between the data from China and Japan and the behavior predicted from the global field models, especially the CALS series. One reason for this might be that the predictions from the models are only based on the published data in the database and the new data are not included. Therefore, we suggest that the global models need to be updated with the new data.

6. Conclusions

In this study, new, reliable, archaeointensity results covering the last 7 kyr are obtained from four locations in eastern China. These fill the gap of archaeomagnetic study in China ever since the systematic work carried out by Wei et al. (1982, 1986, 1987) during the 1980s. Several conclusions can be drawn from our new data set.

1. A newly detected period of paleointensity as low as $\sim 2 \times 10^{22}$ Am^2 (a DIP) at ~2250 BCE, even though based on only two samples, is revealed by our results.
2. A sharp, up to six-fold increase in paleointensity from the DIP at ~2250 BCE to a high field strength at ~1300 BCE with VADM ranging from $\sim 2 \times 10^{22}$ to $\sim 13 \times 10^{22}$ Am^2 is detected. The rate of change of geomagnetic intensity during this period is ~6 μT/century or 47% per century.
3. A possible intensity spike of $\sim 17 \times 10^{22}$ Am^2 at ~200 CE is suggested by the published data from Wei et al. (1982, 1986), which needs further investigation as the data were obtained by methods lacking modern checks.
4. The new data generally agree with the ARCH3k.1 model but deviate significantly from the CALS3k.4 and CALS10k.1b model at certain periods because of the different input data of the models, suggesting that more reliable inputs are necessary to improve the global models.
5. Combining the published data in China and Japan, we provide greatly improved constraints for the regional model of Eastern Asia, which has implications for archaeomagnetic dating in this area in the future.
6. When comparing the Eastern Asian curve with that of two representative areas in the world, the Middle East and Southern Europe, we conclude that the spike in intensity observed in the Middle East around ~1000 BCE may not be global. We prefer to explain the peaks in the three areas as distinct features of the non-dipole field that grow and decay in place as opposed to traveling features of the geomagnetic field caused by migrating flux patches.

Acknowledgements

We thank Limin Wang, Jinghao Yang, Xinmin Xu, Sheng Huang and Shihu Li for sample collection. We thank Jason Steindorf for his help in the laboratory. We thank Ron Shaar for the fruitful and insightful discussions. We thank Greig A. Paterson for the useful discussions during the revision of the manuscript. This study was supported by NSFC1 grants 90814000 and 41274073 awarded to RZ, NSF grant EAR1141840 awarded to LT, CAS Strategic Priority Research Program grant XDA05130603-B awarded to GJ, and the National Key Basic Research Program of China grant 2012CB821900 and NSFC grant 40925012 awarded to CD. The visit of SC to UCSD from September 2011 to August 2012 was supported by the Key Laboratory of the Earth's Deep Interior of CAS. We thank Carlo Laj and two anonymous reviewers for their helpful comments that improved this paper.

Appendix A. Supplementary material

Supplementary material related to this article can be found online at http://dx.doi.org/10.1016/j.epsl.2014.02.030.

References

Aitken, M.J., Alcock, P., Bussell, G.D., Shaw, C., 1981. Archaeomagnetic determination of the past geomagnetic intensity using ancient ceramics: Allowance for anisotropy. Archaeometry 23, 53–64.

Aitken, M.J., Allsop, A.L., Bussell, G.D., Winter, M.B., 1988. Determination of the intensity of the Earth's magnetic field during archeological times: Reliability of the Thellier technique. Rev. Geophys. 26, 3–12.

Amit, H., Korte, M., Aubert, J., Constable, C., Hulot, G., 2011. The time-dependence of intense archeomagnetic flux patches. J. Geophys. Res. 116. http://dx.doi.org/10.1029/2011JB008538.

Bard, E., Delaygue, G., 2008. Comment on "Are there connections between the Earth's magnetic field and climate?" by V. Courtillot, Y. Gallet, J.-L. Le Mouël, F. Fluteau, A. Genevey EPSL 253 (2007) 328. Earth Planet. Sci. Lett. 265, 302–307.

Ben-Yosef, E., Ron, H., Tauxe, L., Agnon, A., Genevey, A., Levy, T.E., Avner, U., Najjar, M., 2008a. Application of copper slag in geomagnetic archaeointensity research. J. Geophys. Res., Solid Earth 113, B08101. http://dx.doi.org/10.1029/2007jb005235.

Ben-Yosef, E., Tauxe, L., Ron, H., Agnon, A., Avner, U., Najjar, M., Levy, T.E., 2008b. A new approach for geomagnetic archaeointensity research: insights on ancient metallurgy in the Southern Levant. J. Archaeol. Sci. 35, 2863–2879. http://dx.doi.org/10.1016/j.jas.2008.05.016.

Ben-Yosef, E., Tauxe, L., Levy, T.E., Shaar, R., Ron, H., Najjar, M., 2009. Geomagnetic intensity spike recorded in high resolution slag deposit in Southern Jordan. Earth Planet. Sci. Lett. 287, 529–539.

Ben-Yosef, E., Tauxe, L., Levy, T.E., 2010. Archaeomagnetic dating of copper smelting site F2 in the Timna Valley (Israel) and its implications for the modelling of ancient technological developments. Archaeometry 52, 1110–1121.

Biggin, A., Steinberger, B., Aubert, J., Suttie, N., Holme, R., Torsvik, T., van der Meer, D., van Hinsbergen, D., 2012. Possible links between long-term geomagnetic variations and whole-mantle convection processes. Nat. Geosci. 5, 526–533.

Bloxham, J., 2000. Sensitivity of the geomagnetic axial dipole to thermal core-mantle interactions. Nature 405, 63–65.

Bloxham, J., Zatman, S., Dumberry, M., 2002. The origin of geomagnetic jerks. Nature 420, 65–68.

Bullard, E.C., Freedman, C., Gellman, H., Nixon, J., 1950. The westward drift of the Earth's magnetic field. Philos. Trans. R. Soc. Lond. A 243, 67–92.

Chauvin, A., Garcia, Y., Lanos, P., Laubenheimer, F., 2000. Paleointensity of the geomagnetic field recovered on archaeomagnetic sites from France. Phys. Earth Planet. Inter. 120, 111–136.

Coe, R.S., 1967. Paleo-intensities of the Earth's magnetic field determined from Tertiary and Quaternary rocks. J. Geophys. Res. 72, 3247–3262.

Coe, R.S., Grommé, S., Mankinen, E.A., 1978. Geomagnetic paleointensities from radiocarbon-dated lava flows on Hawaii and the question of the Pacific nondipole low. J. Geophys. Res., Solid Earth 83, 1740–1756.

Courtillot, V., Gallet, Y., Mouël, J.L., Fluteau, F., Genevey, A., 2007. Are there connections between the Earth's magnetic field and climate?. Earth Planet. Sci. Lett. 253, 328–339.

Cox, A., Hillhouse, J., Fuller, M., 1975. Paleomagnetic records of polarity transitions, excursions, and secular variation. Rev. Geophys. 13, 185–189.

Day, R., Fuller, M., Schmidt, V.A., 1977. Hysteresis properties of titanomagnetites: Grain-size and compositional dependence. Phys. Earth Planet. Inter. 13, 260–267.

Dodson, M.H., McClelland-Brown, E., 1980. Magnetic blocking temperatures of single-domain grains during slow cooling. J. Geophys. Res. 85, 2625–2637.

Donadini, F., Korhonen, K., Riisager, P., Pesonen, L.J., 2006. Database for Holocene geomagnetic intensity information. Eos 87, 137–143.

Dumberry, M., Finlay, C.C., 2007. Eastward and westward drift of the Earth's magnetic field for the last three millennia. Earth Planet. Sci. Lett. 254, 146–157.

Dunlop, D.J., 2002a. Theory and application of the Day plot (Mrs/Ms versus Hcr/Hc) 1. Theoretical curves and tests using titanomagnetite data. J. Geophys. Res. 107. http://dx.doi.org/10.1029/2001JB000486.

Dunlop, D.J., 2002b. Theory and application of the Day plot (Mrs/Ms versus Hcr/Hc) 2. Application to data for rocks, sediments, and soils. J. Geophys. Res. 107. http://dx.doi.org/10.1029/2001JB000487.

Dunlop, D.J., Özdemir, Ö., 1997. Rock Magnetism: Fundamentals and Frontiers. Cambridge University Press, pp. 61–66.

Dunlop, D.J., Xu, S., 1994. Theory of partial thermoremanent magnetization in multidomain grains: I. Repeated identical barriers to wall motion (single microcoercivity). J. Geophys. Res. 99, 9005–9023.

Ertepinar, P., Langereis, C.G., Biggin, A.J., Frangipane, M., Matney, T., Ökse, T., Engin, A., 2012. Archaeomagnetic study of five mounds from Upper Mesopotamia between 2500 and 700 BCE: Further evidence for an extremely strong geomagnetic field ca. 3000 years ago. Earth Planet. Sci. Lett. 357–358, 84–98.

Gallet, Y., Genevey, A., Fluteau, F., 2005. Does Earth's magnetic field secular variation control centennial climate change?. Earth Planet. Sci. Lett. 236, 339–347.
Genevey, A., Gallet, Y., 2002. Intensity of the geomagnetic field in Western Europe over the past 2000 years: new data from French ancient pottery. J. Geophys. Res. 107. http://dx.doi.org/10.1029/2001JB000701.
Gómez-Paccard, M., Chauvin, A., Lanos, P., Dufresne, P., Kovacheva, M., Hill, M.J., Beamud, E., Blain, S., Bouvier, A., Guibert, P., 2012. Improving our knowledge of rapid geomagnetic field intensity changes observed in Europe between 200 and 1400 AD. Earth Planet. Sci. Lett. 355–356, 131–143.
Halgedahl, S.L., Day, R., Fuller, M.D., 1980. The effect of cooling rate on the intensity of weak-field TRM in single-domain magnetite. J. Geophys. Res. 85, 3690–3698.
Hartmann, G.A., Genevey, A., Gallet, Y., Trindade, R.I.F., Le Goff, M., Najjar, R., Etchevarne, C., Afonso, M.C., 2011. New historical archeointensity data from Brazil: Evidence for a large regional non-dipole field contribution over the past few centuries. Earth Planet. Sci. Lett. 306, 66–76.
Hill, M.J., Lanos, P., Denti, M., Dufresne, P., 2008. Archaeomagnetic investigation of bricks from the VIIIth-VIIth century BC Greek-indigenous site of Incoronata (Metaponto, Italy). Phys. Chem. Earth 33, 523–533.
Huang, X.G., Li, D.J., Wei, Q.Y., 1998. Secular Variation of Geomagnetic Intensity for the Last 5000 Years in China-Comparison between the southwest and Other Parts of China. Chin. J. Geophys. 41, 385–396.
Kent, D.V., 1982. Apparent correlation of palaeomagnetic intensity and climatic records in deep-sea sediments. Nature 299, 538–539.
Kent, D.V., Schneider, D.A., 1995. Correlation of paleointensity variation records in the Brunhes/Matuyama polarity transition interval. Earth Planet. Sci. Lett. 129, 135–144.
Kirschvink, J.L., 1980. The least-squares line and plane and the analysis of palaeomagnetic data. Geophys. J. R. Astron. Soc. 62, 699–718.
Kissel, C., Laj, C., 2004. Improvements in procedure and paleointensity selection criteria (PICRIT-03) for Thellier and Thellier determinations: application to Hawaiian basaltic long cores. Phys. Earth Planet. Inter. 147, 155–169.
Korhonen, K., Donadini, F., Riisager, P., Pesonen, L.J., 2008. GEOMAGIA50: An archeointensity database with PHP and MySQL. Geochem. Geophys. Geosyst. 9, Q04029. http://dx.doi.org/10.1029/2007gc001893.
Korte, M., Constable, C., 2011. Improving geomagnetic field reconstructions for 0–3 ka. Phys. Earth Planet. Inter. 188, 247–259.
Korte, M., Donadini, F., Constable, C.G., 2009. Geomagnetic field for 0–3 ka: 2. A new series of time-varying global models. Geochem. Geophys. Geosyst. 10, Q06008. http://dx.doi.org/10.1029/2008gc002297.
Korte, M., Constable, C., Donadini, F., Holme, R., 2011. Reconstructing the Holocene geomagnetic field. Earth Planet. Sci. Lett. 312, 497–505.
Livermore, P.W., Fournier, A., Gallet, Y., 2014. Core-flow constraints on extreme archeomagnetic intensity changes. Earth Planet. Sci. Lett. 387, 145–156.
Mandea, M., Holme, R., Pais, A., Pinheiro, K., Jackson, A., Verbanac, G., 2010. Geomagnetic jerks: rapid core field variations and core dynamics. Space Sci. Rev. 155, 147–175.
Mitra, R., Tauxe, L., McIntosh, S.K., 2013. Two thousand years of archeointensity from West Africa. Earth Planet. Sci. Lett. 364, 123–133.
Nagata, T., Arai, Y., Momose, K., 1963. Secular variation of the geomagnetic total force during the last 5000 years. J. Geophys. Res. 68, 5277–5281.
Olsen, N., Mandea, M., 2008. Rapidly changing flows in the Earth's core. Nat. Geosci. 1, 390–394.
Paterson, G.A., 2013. The effects of anisotropic and non-linear thermoremanent magnetizations on Thellier-type paleointensity data. Geophys. J. Int. 193. http://dx.doi.org/10.1093/gji/ggt1033.
Pavón-Carrasco, F.J., Osete, M.L., Torta, J.M., Gaya-Piqué, L.R., 2009. A regional archeomagnetic model for Europe for the last 3000 years, SCHA.DIF.3K: Applications to archeomagnetic dating. Geochem. Geophys. Geosyst. 10, Q03013. http://dx.doi.org/10.1029/2008gc002244.
Pavón-Carrasco, F.J., Rodríguez-González, J., Osete, M.L., Torta, J.M., 2011. A Matlab tool for archaeomagnetic dating. J. Archaeol. Sci. 38, 408–419.
Roberts, A.P., Pike, C.R., Verosub, K.L., 2000. First-order reversal curve diagrams: A new tool for characterizing the magnetic properties of natural samples. J. Geophys. Res., Solid Earth 105, 28461–28475.
Rogers, J., Fox, J.M.W., Aitken, M.J., 1979. Magnetic anisotropy in ancient pottery. Nature 277, 644–646.
Selkin, P.A., Meurer, W.P., Newell, A.J., Gee, J.S., Tauxe, L., 2000. The effect of remanence anisotropy on paleointensity estimates: A case study from the Archean Stillwater Complex. Earth Planet. Sci. Lett. 183, 403–416.
Shaar, R., Tauxe, L., 2013. Thellier GUI: An integrated tool for analyzing paleointensity data from Thellier-type experiments. Geochem. Geophys. Geosyst. 14, 677–692.
Shaar, R., Ron, H., Tauxe, L., Kessel, R., Agnon, A., Ben-Yosef, E., Feinberg, J.M., 2010. Testing the accuracy of absolute intensity estimates of the ancient geomagnetic field using copper slag material. Earth Planet. Sci. Lett. 290, 201–213.
Shaar, R., Ben-Yosef, E., Ron, H., Tauxe, L., Agnon, A., Kessel, R., 2011. Geomagnetic field intensity: How high can it get? How fast can it change? Constraints from Iron Age copper slag. Earth Planet. Sci. Lett. 301, 297–306.
Shaw, J., Yang, S., Wei, Q.Y., 1995. Archaeointensity variations for the past 7500 years evaluated from ancient Chinese ceramics. J. Geomagn. Geoelectr. 47, 59–70.
Shaw, J., Yang, S., Rolph, T.C., Sun, F.Y., 1999. A comparison of archaeointensity results from Chinese ceramics using microwave and conventional Thellier's and Shaw's methods. Geophys. J. Int. 136, 714–718.
Tang, C., Zheng, J.Y., Li, D.J., Wei, S.F., Wei, Q.Y., 1991. Paleointensity determinations for the Xinjiang Region, NW China. J. Geomagn. Geoelectr. 43, 363–368.
Tauxe, L., Staudigel, H., 2004. Strength of the geomagnetic field in the Cretaceous Normal Superchron: New data from submarine basaltic glass of the Troodos Ophiolite. Geochem. Geophys. Geosyst. 5, Q02H06. http://dx.doi.org/10.1029/2003GC000635.
Tauxe, L., Mullender, T.A.T., Pick, T., 1996. Potbellies, wasp-waists, and superparamagnetism in magnetic hysteresis. J. Geophys. Res., Solid Earth 101, 571–583.
Tauxe, L., Butler, R., Banerjee, S.K., van der Voo, R., 2010. Essentials of Paleomagnetism. University of California Press, Berkeley, pp. 69–72.
Tema, E., Gomez-Paccard, M., Kondopoulou, D., Almar, Y., 2012. Intensity of the Earth's magnetic field in Greece during the last five millennia: New data from Greek pottery. Phys. Earth Planet. Inter. 202–203, 14–26.
Thellier, E., Thellier, O., 1959. Sur l'intensité du champ magnétique terrestre dans le passé historique et géologique. Ann. Geophys. 15, 285–378.
Vandamme, D., 1994. A new method to determine paleosecular variation. Phys. Earth Planet. Inter. 85, 131–142.
Veitch, R.J., Hedley, I.G., Wagner, J.J., 1984. An investigation of the intensity of the geomagnetic field during Roman times using magnetically anisotropic bricks and tiles. Arch. Sci. (Geneva) 37, 359–373.
Vestine, E.H., Kahle, A.B., 1968. The westward drift and geomagnetic secular change. Geophys. J. R. Astron. Soc. 15, 29–37.
Wei, Q.Y., Li, D.J., Cao, G.Y., Zhang, W.S., Wang, S.P., 1982. Intensity of the geomagnetic field near Loyang, China between 500 BC and AD 1900. Nature 296, 728–729.
Wei, Q.Y., Li, D.J., Cao, G.Y., Zhang, W.X., Wei, S.F., 1986. The total intensity of geomagnetic field in southern China for the period from 4500 B.C. to A.D. 1500. J. Geomagn. Geoelectr. 38, 1311–1322.
Wei, Q.Y., Zhang, W.X., Li, D.J., Aitken, M.J., Busseil, G.D., Winter, M., 1987. Geomagnetic intensity as evaluated from ancient Chinese pottery. Nature 328, 330–333.
Xu, S., Dunlop, D.J., 1994. Theory of partial thermoremanent magnetization in multidomain grains: II. Effect of microcoercivity distribution and comparison with experiment. J. Geophys. Res. 99, 9025–9033.
Yu, Y.J., 2012. High-fidelity paleointensity determination from historic volcanoes in Japan. J. Geophys. Res., Solid Earth 117, B08101. http://dx.doi.org/10.1029/2012jb009368.
Yu, Y.J., Tauxe, L., 2005. Testing the IZZI protocol of geomagnetic field intensity determination. Geochem. Geophys. Geosyst. 6, Q06H11. http://dx.doi.org/10.1029/2004GC000840.
Yu, Y.J., Tauxe, L., Genevey, A., 2004. Toward an optimal geomagnetic field intensity determination technique. Geochem. Geophys. Geosyst. 5, Q02H07. http://dx.doi.org/10.1029/2003GC000630.